Astronomy &Astrophysics

Near-infrared observations of galaxies in Pisces-Perseus

V. On the origin of bulges[*]

L. K. Hunt[1], D. Pierini[2], and C. Giovanardi[3]

[1] Istituto di Radioastronomia-Firenze/CNR, Largo E. Fermi 5, 50125 Firenze, Italy
  e-mail: hunt@arcetri.astro.it
[2] Max-Planck-Institut für extraterrestrische Physik (MPE), Giessenbachstrasse, 85748 Garching, Germany
  e-mail: dpierini@mpe.mpg.de
[3] INAF-Osservatorio Astrofisico di Arcetri, Largo E. Fermi 5, 50125 Firenze, Italy
  e-mail: giova@arcetri.astro.it

Abstract. We investigate the scaling relations of bulge and disk structural parameters for a sample of 108 disk galaxies. Structural parameters of individual galaxies are obtained from two-dimensional bulge/disk decomposition of their H-band surface brightness distributions[**]. Bulges are modelled with a generalized exponential (Sérsic) with variable integer shape index n. We find that bulge effective scalelengths r_e^B and luminosity M^B increase with increasing n, but disk properties are independent of bulge shape. As Hubble type T increases, bulges become less luminous and their mean effective surface brightness $< \mu_e^B >$ gets fainter; disk $< \mu_e^D >$ shows a similar, but much weaker, trend. When bulge parameters ($< \mu_e^B >$, r_e^B, M^B) are compared with disk ones ($< \mu_e^D >$, r_e^D, M^D), *they are tightly correlated for $n = 1$ bulges*. The correlations gradually worsen with increasing n such that $n = 4$ bulges appear *virtually independent* of their disks. The Kormendy relation, $< \mu_e^B >$ vs. r_e^B, is shown to depend on bulge shape n; the two parameters are tightly correlated in $n = 4$ bulges ($r = 0.8$), and increasingly less so as n decreases; disk $< \mu_e^D >$ and r_e^D are well correlated ($r = 0.7$). Bulge-to-disk size ratios r_e^B/r_e^D are independent of Hubble type, but smaller for exponential bulges; the mean r_e^B/r_e^D for $n = 1$ bulges is 4 times smaller than that for $n = 4$, with a spread which is 9 times smaller. Strongly barred SB galaxies with exponential bulges are more luminous than their unbarred counterparts. Exponential bulges appear to be closely related to their underlying disks, while bulges with higher n values are less so; $n = 4$ bulges and their disks apparently have no relation. We interpret our results as being most consistent with a secular evolutionary scenario, in which dissipative processes in the disk are responsible for building up the bulges in most spirals.

Key words. galaxies: evolution – galaxies: formation – galaxies: fundamental parameters – galaxies: spiral – galaxies: structure – infrared: galaxies

1. Introduction

This is the fifth paper in a series based on near-infrared imaging of a sample of disk galaxies in the Pisces-Perseus supercluster. Already in Paper III of the series (Moriondo et al. 1999b), we explored the relations between structural parameters of bulges and disks, but in the context of distance measurements and the consequent definition of their Fundamental Planes. For this reason, that paper: *i)* made only use of the subset of galaxies (40) with measured rotation curves, and *ii)* postponed to future work the discussion of the impact of scaling relations of bulges and disks on their formation and evolution. In the present paper, we will address this issue.

The traditional picture is that bulges formed well before the disk of a galaxy, in a "monolithic collapse", either as the first rapid stage of the collapse of a galaxy-size density perturbation, as in the Milky Way collapse model of Eggen et al. (1962), or through the infall of enriched gas from the star-forming halo (Carney et al. 1990). "Early" bulge formation is also predicted within the framework of hierarchical cold-dark matter (CDM) scenarios of structure formation and evolution (Kauffmann et al. 1993; Baugh et al. 1996). In this case, the bulge originates from the merging of stellar disks within the merging halos, while the disk that is observed today is assembled through gas accretion at later epochs. A more recent variation of this scenario is the growth of galactic bulges through merging of dense satellites (Aguerri et al. 2001). Evidence in favor of "early" bulge formation rises from studies of the stellar populations in the Milky-Way bulge (Ortolani et al. 1995) and in bulges of nearby galaxies (Jablonka et al. 1996). In addition, bulge velocity fields

(Kormendy & Illingworth 1982) and their high central surface brightness seem to be imprints of a formation process that involved dissipational collapse (e.g., Carlberg 1986) at epochs earlier than the formation of the disks and, perhaps, of the stellar halo.

More recently, it has been suggested that the bulges in (some) disk galaxies can be formed after the disk, through secular evolutionary phenomena. Numerical simulations (Combes & Sanders 1981; Combes et al. 1990; Norman et al. 1996) have shown that a spheroidal stellar component can originate from dissipationless processes such as the thickening or destruction of a bar. Moreover, when gas is included in the simulations, dissipation accelerates the evolution, giving rise to galaxies which are more centrally concentrated (Junqueira & Combes 1996). Indeed, some of the observed bulge characteristics such as triaxial or peanut shape and cylindrical rotation (e.g., Shaw 1993; Lütticke et al. 2000) are predicted by such models. However, gas is not necessary for dissipation, as pointed out by Zhang in a series of papers (Zhang 1996, 1998, 1999). Secular evolution may also operate through outward transport of angular momentum through a collective dissipative process linked to spiral density waves. Observational evidence in favor of the secular scenario include the similarity of bulge and disk color indices (e.g., Balcells & Peletier 1994), the mass-to-luminosity ratios of the components (Widrow et al. 2003), the disk-like kinematics observed in many bulges (Kormendy 1993), and the correlation of bulge and disk scalelengths (de Jong 1996). Indeed, when a simple exponential is used to fit the bulge surface brightness profile, a strong correlation is found between bulge and disk scalelengths (Courteau et al. 1996), seemingly supporting the secular formation scenario for bulges. The correlation was later shown to depend critically on the use of a simple exponential as a bulge fitting function, since when generalized exponentials were used instead, the mean scalelength ratio depends on the bulge shape index (Moriondo et al. 1998a – hereafter MGH; Graham & Prieto 1999). Thus it appears, albeit for small samples, that the ratio of bulge and disk scalelengths may not be constant over a range of Hubble types as previously claimed. This is of importance not only for the chronology of bulge and disk formation, but also for the meaning of the Hubble sequence itself in terms of photometric observables (scale-free Hubble sequence).

To further investigate bulge and disk structural parameters, and to better constrain their connection with formation scenarios, we have performed two-dimensional (2D) bulge/disk decompositions on a large sample of disk galaxies in the Pisces Perseus supercluster (see Moriondo et al. 1999a, hereafter Paper I). These decompositions are performed on image data in the H band because the near-infrared (NIR) wavelengths are the most direct tracer of the stellar mass (e.g., Rix & Rieke 1993; Gavazzi 1993). Moreover, NIR emission is much less affected by recent episodes of star formation which typically dominate disk morphology at optical wavelengths. Finally, the effects of dust extinction are mitigated at $1.65\,\mu$m (H) since A_H is roughly a factor of 8 lower than A_V. We describe the sample and the imaging data in Sect. 2, together with the bulge/disk decompositions. Section 3 presents our results, and we

interpret them in Sect. 4 in the context of various evolutionary scenarios.

2. The sample, the images, and the structural decomposition

The galaxies under investigation belong to a sample selected from the catalogued disk galaxies in the Pisces-Perseus (PP) supercluster area, $22^h < RA < 4^h$ and $0° < \delta < 45°$, excluding obvious foreground members with heliocentric velocities less than 3000 km s^{-1}. The original sample was restricted to about 950 galaxies with optical major axis $0\!'\!5 < a < 4\!'\!0$ and available good-quality 21-cm spectra (Giovanelli & Haynes 1989 and references therein). From this set two distinct subsamples were extracted. Sample A comprises about 150 galaxies, randomly selected to cover the entire area and inclination range, and with types Sb or later. Sample B comprises the 50 cluster galaxies within an angular distance of 5.5° from the Pisces cluster center (1^h20^m, 33°), with optical size $a \geq 0\!'\!8$ and inclination $30° < i < 75°$, spanning the range S0 to Sd in Hubble type.

Out of these 200 objects, images were obtained for 174 galaxies (see Paper I) in the H band (35 in JHK) with the ARNICA camera (Lisi et al. 1993, 1996; Hunt et al. 1996) mounted on various telescopes. We refer the reader to Paper I for details concerning observations, data reduction, and photometric calibration. Analysis of the JHK color images is presented in Moriondo et al. (2001, Paper IV). Unless otherwise specified, all the photometric data derived and here reported refer to the set of images in the H band.

2.1. Two-dimensional bulge/disk decomposition

As in MGH, we fitted the images with a two-dimensional (2D) parametric brightness distribution model, consisting of a generalized exponential (Sèrsic 1968) bulge of shape index n:

$$I^B(x,y) = I_e \exp\left\{-\alpha_n\left[\left(\frac{1}{r_e}\sqrt{x^2 + \frac{y^2}{(1-\epsilon^B)^2}}\right)^{1/n} - 1\right]\right\}, \quad (1)$$

and an exponential thin disk:

$$I^D(x,y) = I_d(0)\exp\left[-\frac{1}{r_d}\sqrt{x^2 + \frac{y^2}{\cos^2 i}}\right]. \quad (2)$$

I_e and r_e are effective (half-light) values, ϵ^B is the apparent bulge ellipticity, α_n is a constant relating the effective brightness and radius to the exponential values (see MGH). x and y are in arbitrary units, with origin at the galaxy's center, and x along the major axis. The bulge is assumed to be an oblate rotational ellipsoid (Kent et al. 1991), coaxial with the disk, and its apparent eccentricity e^B is related to the intrinsic eccentricity e'^B by:

$$e^B = e'^B \sin i. \quad (3)$$

The structural parameters have been determined by fitting the 2D image to the model, convolved with a circular Gaussian seeing disk of appropriate $FWHM$, using a χ^2 minimization. The parameters left free to vary in the fit include: the two surface
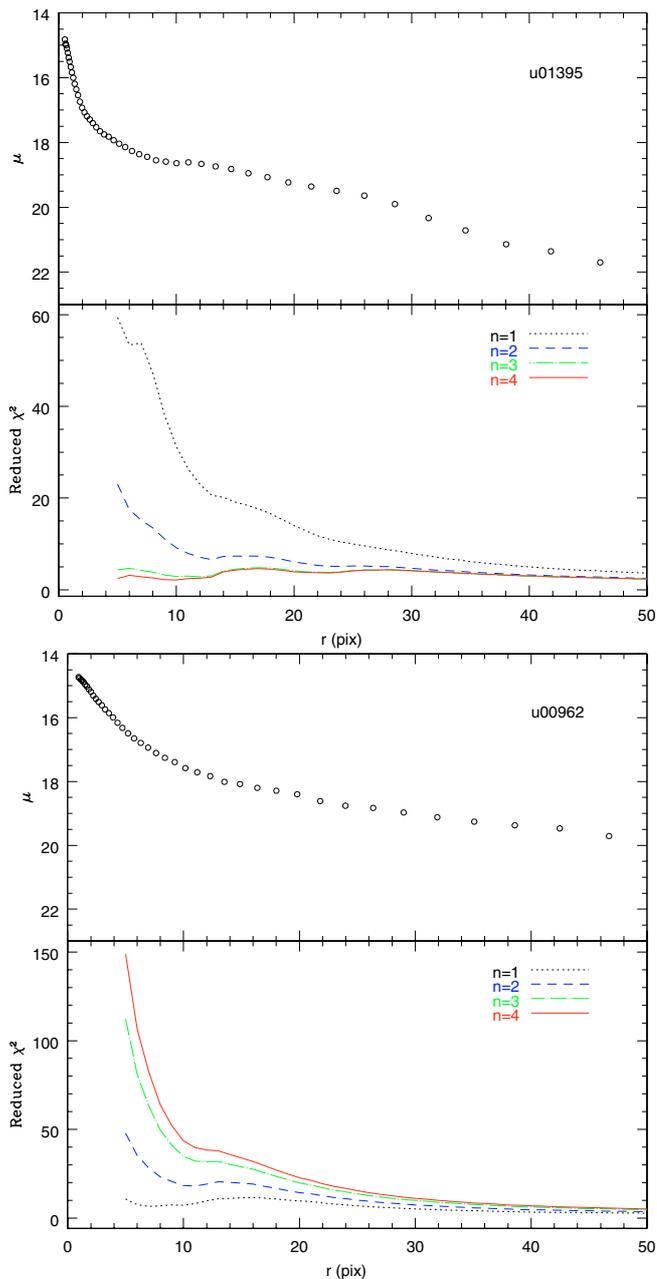
Fig. 1. *Upper panels*: surface brightness profile along the major axis (from elliptical isophotal fitting) in H mag arcsec^{-2}. *Lower panels*: radial run of the reduced χ^2 of the best-fitting 2D model for different values of the n. The first panel shows a galaxy with a best-fit n of 4, while a best-fit $n = 1$ is shown in the second panel. Abscissas are labelled in pixel, 1 pixel = 0.975 arcsec.

brightnesses I_e and $I_d(0)$ (or μ_e and μ_0 when given in magnitudes), the two scale lengths r_e and r_d, the bulge ellipticity ϵ^B, and the system inclination i. The fitting algorithm and tests of its reliability are described more fully in MGH.

The use of a 2D fitting technique is mandatory in the analysis of objects of middle to high inclination, such as samples – including the present one (68 galaxies with $i > 40°$) – selected for Tully-Fisher studies. A feature of our algorithm is its ability to suppress non-axisymmetric structure. This is achieved through a "folding" procedure in which we exploit the model symmetry about the major and minor axes. The galaxy image

is first "folded" about the major axis (measured a priori), in order to obtain the "long" semi-ellipse; it is then folded again about the minor axis in order to obtain only one quadrant. There are consequently four points used to infer the value of a single pixel in the folded quadrant, and from these, a mean and a standard deviation are calculated; only this single quadrant is input to the fitting routine. Typically pixels are weighted by the photon statistics, calculated by modelling the detector noise characteristics and assuming background limited performance (verified to be true in all cases). The weighting scheme however gives greater weight to those regions with low standard deviation since it chooses the maximum of the Poisson statistics or the standard deviation resulting from the folding procedure. The regions with significant asymmetry show up with large standard deviation in the folding process, and they are given accordingly less weight in the decomposition.

Because of the known mutual functional dependency of r_e, μ_e, and n, we chose to use a "grid method" for the determination of n rather than include it as a free parameter (see also MacArthur et al. 2003, hereafter MACH03). Because of the large sample and consequent numerical calculation time for the 2D fits, we restricted n to integer values of 1, 2, 3 or 4, and ran fits for each of these separately. The best-fitting n value was then derived by minimizing the reduced χ^2 over the inner region. Two examples of the radial run of χ^2_ν for different n's are shown in Fig. 1. The surface brightness profiles in the upper panels are derived from elliptical isophotal fitting and are only used for display purposes; the lower panels show the behavior of the reduced χ^2 resulting from the 2D best fit at different n, averaged within the same elliptical annuli of the upper panel. As can be seen, the bulge fit influences primarily the inner part of the galaxy. It is consequently necessary to consider the value of χ^2_ν as a function of n especially at small radii, because the large area of the disk tends to make the influence of the bulge shape in the global χ^2 very small and easily masked by other features. The median (and mean) *FWHM* seeing of the images in our database is 1″.9. Only 4 of 108 galaxies have r_e^B smaller than this, but it is difficult to distinguish star clusters or nuclear point sources from high-n bulges. Point sources have not been included in our fits.

The discretized range of integer n values 1, 2, 3, 4 samples rather well the continuous range of n values found by previous authors. MACH03, on the basis of one-dimensional (1D) profile fits, conclude that the surface brightness profiles of Freeman type-I galaxies (Freeman 1970) are adequately described by a double-exponential distribution with bulges of $0.1 < n < 2$. However this sample consists of late types ($T \geq 3$); only 8 of their objects have $n < 0.5$. On the other hand, with 2D fits, Möllenhoff & Heidt (2002, hereafter MH01) found bulge shape indices of $0.8 < n < 6.7$ for their sample of 40 bright galaxies, with only one object having a bulge with $n < 1$ and two objects with $n > 4$.

The fits were judged to be reliable ($\chi^2_\nu \leq 2$) in 117 (of 174) galaxies. The average percentage errors for the fitted parameters of bulge and disk are less than 20%, consistent with MH01 and MACH03. We have further restricted the final database to contain only those galaxies with apparent optical diameter

$a \geq 1'$ (from NED[1]). Thus, the final PP sample consists of 108 galaxies, 2 of which do not have well-defined morphological types, and to which we have assigned $T = 5$ (following LEDA, the Extragalactic Database based in Lyon). The best fit parameters resulting from our 2D fits for these 108 disk galaxies are reported in Table 1. Distances to individual galaxies are determined from the Hubble law (with $H_0 = 70 \text{ km s}^{-1} \text{ Mpc}^{-1}$) after correcting the heliocentric radial velocities listed in Paper I to the CMB reference frame according to the prescription of the Third Reference Catalogue (de Vaucouleurs et al. 1991, hereafter RC3). The full table is only available in electronic form at the CDS, please see the footnote to the Abstract, here we reproduced it partly to illustrate its contents. Table 1 also contains additional information from RC3 as follows:

Column 1: UGC galaxy number, if not differently specified;
Column 2: distance (Mpc);
Column 3: Hubble type T;
Column 4: bar class;
Column 5: global χ_ν^2 of fit;
Column 6: bulge shape index n ($n = 0$ for pure disks);
Column 7: apparent bulge ellipticity ϵ^B;
Columns 8, 9: bulge effective radius r_e and uncertainty (arcsec);
Columns 10, 11: bulge effective surface brightness, reduced to face-on, μ_e and uncertainty (mag arcsec^{-2});
Column 12: total bulge apparent magnitude m^B (mag);
Column 13: disk inclination i (degrees);
Columns 14, 15: disk scalelength r_d and uncertainty (arcsec);
Columns 16, 17: central face-on disk surface brightness μ_0 (and uncertainty mag arcsec^{-2});
Column 18: total disk apparent magnitude m^D (mag);
Column 19: bulge-to-disk luminosity ratio B/D;
Column 20: total galaxy apparent magnitude m (mag).

2.2. Photometric corrections

The magnitudes have been corrected for Galactic extinction according to the estimates given by Burstein & Heiles (1984) as reported by NED, and assuming the extinction curve of Cardelli et al. (1989). Using the recipe of Frogel et al. (1978), we have applied corrections for redshift dimming.

While internal dust extinction may affect the estimates of structural parameters even in the NIR (e.g., Peletier & Willner 1992), the corrections are small and subject to some uncertainty. An empirical analysis of the photometric corrections for dust extinction in this sample has been carried out by Moriondo et al. (1998b, hereafter Paper II). To do this, they rely on correlations with inclinations of the observed disk and bulge structural parameters and colors, and find that the structural parameters of the bulge are not affected by dust extinction, while those of the disk may be – especially the disk scalelength – but with large scatter. However, the analysis Paper II is based on the assumption that dust is homogeneously distributed within a thin disk coincident with the mid-plane of the stellar distribution, which in general is not true (e.g. Bianchi et al. 1996,

2000; Ferrara et al. 1999). Moreover, the behavior of the kinematic scalelength as a function of the axial ratio is complex (Giovanelli & Haynes 2002, see also Paper II). Therefore, for the subsequent analysis, the structural parameters (r_e, μ_e, m^B, r_d, μ_0, m^D, B/D and m) are corrected to face-on assuming full transparency, which implies no corrections to scalelengths, total magnitudes, and bulge-to-disk luminosity ratio B/D.

All the above corrections have already been applied to the data reported in Table 1.

2.3. Comparison with previous work

Our sample contains five galaxies (UGC 463, UGC 927, UGC 1089, UGC 12378, UGC 12527) in common with MACH03 (H band). In all cases, the two sets of disk parameters agree quite well: r_d(ours)/r_d(theirs) = 0.95 ± 0.05 and μ_0(ours)-μ_0(theirs) = 0.16 ± 0.06 H-mag arcsec^{-2}. For UGC 927, they classify their profile as a "truncated disk", but it appears very different from our major-axis cut (all our fits can be obtained in graphic form by request from the authors). They find $n = 2.7$, the largest in their sample, while we find $n = 4$; the bulge surface brightnesses differ by about ~ 1 mag. This may be an example of the pitfalls of 1D fitting since this galaxy has twisted isophotes, and marked spiral structure even in the NIR. Such morphological features tend to be suppressed by our fitting algorithm, and the greater number of degrees of freedom in 2D image fitting is clearly an advantage.

In general, we find larger n values than those by MACH03: the mean difference $\Delta n = 1.1 \pm 0.75$. We also find larger bulge r_e, but this is expected because of the different n's. This may be another advantage of our fitting algorithm, as it takes into account the non-spherical shape of the bulge (e.g., MGH). Bulges are rarely spherical (Kent 1988), and not considering the possible bulge ellipticity would result in a steeper bulge outer profile, and thus a lower n.

3. Results

A priori the parent sample suffers from a known dearth of early-type spirals (e.g., $T \leq 2$, see Paper I). Indeed our present sample contains only 6 galaxies with type Sab or earlier, with a sample median of $T = 5$ (Sc). Therefore, we have added to the subsequent analysis the sample of 14 early-type spirals (Sa's) studied by MGH; the same fitting algorithm was used to decompose the images[2]. The combined sample comprises 122 galaxies, now with 21 of type Sab or earlier, and with median $T = 4$ (Sbc).

Throughout the analysis, we will make use of mean effective surface brightnesses (SFBs), calculated as the average flux within a circular area of radius r_e. The disk scalelengths r_d are converted to effective ones r_e^D by multiplying by a factor of 1.6784 appropriate for $n = 1$ (see MGH), and we define the mean effective SFB $< \mu_e^B >$ and $< \mu_e^D >$ for bulge and disk respectively. In the following, to avoid confusion, the bulge scalelength will be indicated as r_e^B. Mean SFBs $< \mu_e >$ were chosen, rather than the central μ_0 (Khosroshahi et al. 2000a, 2000b), or

---

[1] The NASA/IPAC Extragalactic Database (NED) is operated by the Jet Propulsion Laboratory, California Institute of Technology, under contract with the National Aeronautics and Space Administration.

[2] A correction of 0.25 mag has been made to convert the K-band quantities in that paper to the H band used here (e.g., Giovanardi & Hunt 1996). The distance scale has also been transformed to the H_0 ($70 \text{ km s}^{-1} \text{ Mpc}^{-1}$) adopted for this study.

Table 1. Galaxy parameter.

UGC (1)	Dist. (2)	T (3)	Bar (4)	χ^2_ν (5)	n (6)	ϵ^B (7)	r_e (8)	(9)	μ_e (10)	(11)	m^B (12)	i (13)	r_d (14)	(15)	μ_0 (16)	(17)	m^D (18)	B/D (19)	m (20)
IC1669	82	1	none	1.0	1	0.62	0.8	0.1	19.18	0.28	16.89	71	7.0	0.1	18.45	0.03	12.22	0.01	12.20
14	103	5	none	1.3	1	0.27	1.5	0.1	16.77	0.07	13.16	44	9.7	0.4	17.91	0.05	10.98	0.13	10.84
26	71	3	SB	1.8	2	0.16	3.3	0.1	18.09	0.02	12.44	56	21.1	1.0	19.76	0.06	11.14	0.30	10.86
57	65	3	SA	1.0	2	0.14	5.0	0.1	16.80	0.01	10.26	44	29.3	2.1	19.46	0.09	10.14	0.89	9.44
60	72	3	none	1.0	2	0.00	2.1	0.4	17.53	0.16	12.85	76	10.7	0.2	17.53	0.03	10.38	0.10	10.28
74	56	5	SAB	1.4	1	0.15	1.5	0.1	17.80	0.04	14.20	33	12.2	0.1	17.86	0.01	10.43	0.03	10.40
98	68	4	SB	1.8	2	0.06	1.7	0.7	17.72	0.38	13.54	54	7.8	0.3	17.34	0.08	10.87	0.09	10.78
100	71	4	SAB	1.2	2	0.08	2.4	0.2	17.24	0.06	12.35	64	12.1	0.3	18.08	0.05	10.68	0.21	10.46
214	77	5	SAB	1.2	4	0.17	2.2	0.2	16.27	0.12	11.17	41	11.1	0.3	17.22	0.05	10.00	0.34	9.68
230	76	6	none	1.4	2	0.00	16.8	1.4	20.33	0.07	11.17	84	41.6	10.6	22.85	0.37	12.76	4.32	10.95
301	76	4	SAB	1.7	4	0.26	3.3	1.1	18.64	0.43	12.67	44	10.5	0.3	17.53	0.07	10.43	0.13	10.30
311	92	6	none	1.6	3	0.04	7.2	0.4	19.25	0.04	11.72	17	10.7	0.6	19.02	0.14	11.87	1.15	11.04
365	66	2	SA	1.0	3	0.43	9.9	0.2	18.13	0.01	9.91	81	12.3	0.3	18.28	0.07	10.85	2.37	9.53
380	75	4	SB	1.2	2	0.24	3.0	0.1	17.36	0.03	11.96	45	16.3	0.2	17.87	0.02	9.81	0.14	9.67
420	74	4	SB	1.4	4	0.23	3.8	0.8	18.25	0.26	11.98	59	15.6	0.5	17.95	0.06	9.99	0.16	9.83
438	65	5	SAB	1.1	4	0.30	20.2	0.9	19.85	0.04	9.93	47	11.4	0.1	17.34	0.03	10.06	1.13	9.24
448	69	5	SAB	2.0	4	0.21	6.7	0.7	18.79	0.11	11.29	39	16.6	1.5	19.07	0.17	10.97	0.75	10.37
462	80	5	SAB	1.2	1	0.06	1.1	0.1	16.92	0.04	14.10	20	10.4	0.2	18.04	0.02	10.96	0.06	10.90
463	64	5	SAB	1.4	1	0.00	2.1	0.1	16.98	0.05	12.63	0	11.9	0.2	17.15	0.04	9.78	0.07	9.71
493	75	6	none	1.1	1	0.22	2.5	0.1	16.69	0.03	11.96	50	13.1	0.3	17.48	0.03	9.90	0.15	9.75
673	89	5	SA	0.9	2	0.46	1.1	0.6	20.00	0.73	16.73	59	5.8	1.8	18.44	0.60	12.64	0.02	12.61
690	84	6	none	1.1	1	0.14	1.4	0.2	17.75	0.17	14.38	44	12.8	0.5	18.25	0.04	10.71	0.03	10.67
710	178	4	none	0.9	2	0.45	2.6	0.1	18.55	0.05	13.46	75	7.5	0.2	18.23	0.04	11.87	0.23	11.64
714	66	5	SA	1.6	3	0.00	1.1	0.2	18.50	0.18	15.05	49	11.7	0.1	18.37	0.02	11.03	0.02	11.00
725	72	6	SB	1.1	2	0.12	2.1	0.7	19.48	0.29	14.79	77	14.4	0.4	18.90	0.04	11.11	0.03	11.07
728	70	5	SAB	1.2	2	0.40	15.0	2.1	21.11	0.12	12.20	55	102.5	18.2	20.63	0.11	8.58	0.04	8.54
732	78	7	SA	1.1	2	0.41	1.5	0.3	18.93	0.31	15.07	55	9.6	0.2	18.10	0.03	11.21	0.03	11.18
738	65	8	none	0.9	1	0.04	2.8	0.2	20.07	0.07	15.18	16	11.0	0.4	18.99	0.05	11.80	0.04	11.75

μ_e – the SFB at r_e (e.g., Graham 2001; MACH03) – because of the strong functional dependence on n of the latter parameters. If a given bulge is fit with a generalized exponential, μ_e becomes fainter as n of the fit becomes larger, because of the mathematical form of the generalized exponential. Higher n fits are more strongly peaked and consequently have a higher μ_0, but are more extended, hence a larger r_e, a fainter μ_e, and a higher bulge luminosity M^B (cf., Fig. 2 in MGH). In practice, when the same bulge is fit with n varying between 1 and 4, the resulting μ_e changes typically by more than 3 mag arcsec^{-2}, while $< \mu_e >$ also becomes fainter but by $\lesssim 1$ mag arcsec^{-2}. The adoption of $< \mu_e >$ also conforms to the definitions of RC2 and RC3, and to all the lore of the Fundamental Plane (FP).

3.1. Pure disk galaxies

Only two of the galaxies (UGC 975 and UGC 1579) are best fit with pure disks ($B/D = 0$); bulges are found in all the others, although in some cases as faint as 16.9 H mag, with B/D ratios of 1%. UGC 975 is classified as a generic spiral ("S"), as it shows on blue images a tight flocculent pattern and high surface brightness. UGC 1579, an almost face-on SB(s)d, shows an extended spiral structure and a large central region of relatively high surface brightness. They are among the faintest objects in the sample, but still galaxies with $M \sim -22$ H mag, and are not low surface brightness galaxies. Pure disks are rare in our sample, although it comprises 50 galaxies with $T \geq 5$. The selection criteria adopted tend to avoid very late types of low surface brightness; for this reason, our two pure disks are unlikely to be representative of their class (cf. Gavazzi et al. 2000).

3.2. Possible biases

In principle, the performance of our decomposition procedure could depend on the size and quality of the image. We have performed a simple check for such biases by examining the distributions of apparent galaxy parameters versus the bulge shape index n, as shown in Fig. 2; optical properties are taken from RC3. The only evidence is that: (*i*) the two pure-disk ($n = 0$) galaxies are faint, and (*ii*) the Sa's from MGH are substantially brighter than the PP set. For the rest, no obvious significant trends are detectable. In particular, we observe no trend for faint, small, and highly inclined galaxies, that is those observed with lower relative resolution, to be better fit with any particular n values. This is important for the reliability of any assertions regarding trends with bulge shape index.

3.3. Hubble type and bulge shape n

The upper panel of Fig. 3 shows the distribution of Hubble types T for our combined sample. The PP and MGH samples have different shadings and the paucity of early-type spirals in the original PP sample is evident.

The lower panel shows the means of the bulge shape index n averaged over different Hubble types. Here and in the following we have grouped Hubble types into four bins: $T \leq 2$, $2 < T \leq 4$, $4 < T \leq 6$, and $T \geq 7$. It can be seen from the figure that $n = 1$ bulges tend to be more common in later-type spirals, and that early types ($T \leq 2$) tend to have bulges with
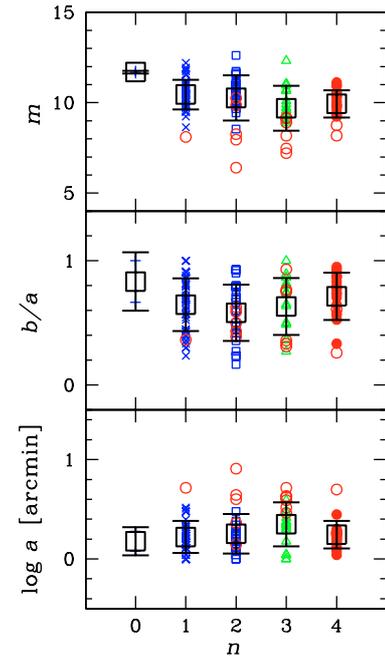

Fig. 2. Distributions of H-band apparent magnitude m (top panel), optical axial ratio b/a (middle), and apparent optical size a (lower) as a function of bulge shape index n. Galaxies best fitted with $n = 1, 2, 3, 4$ are shown by $\times$, open squares, open triangles, and filled circles, respectively. The early-type spirals from MGH are also included and shown as open circles independently of their n. Data for pure-disk galaxies are shown by $+$ at $n = 0$. Large open squares correspond to mean values, and the error bars to 1σ standard deviation.
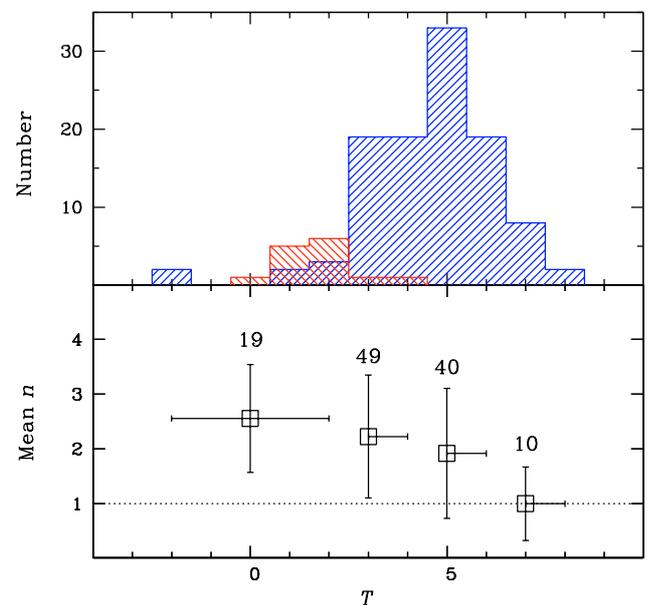

Fig. 3. Distribution of Hubble type T (upper panel) and bulge shape index n versus T (lower panel). In both panels, as in all subsequent figures, the galaxies from MGH are included. In the histogram, the shading for the PP sample is right slanted and for the MGH sample is left slanted. In the lower panel, horizontal error bars indicate the range of Hubble type over which the mean n is calculated. The vertical bars are 1σ standard deviation. The horizontal dotted line is placed at $n = 1$ for convenience. The number of objects in each T bin is printed over its data point.
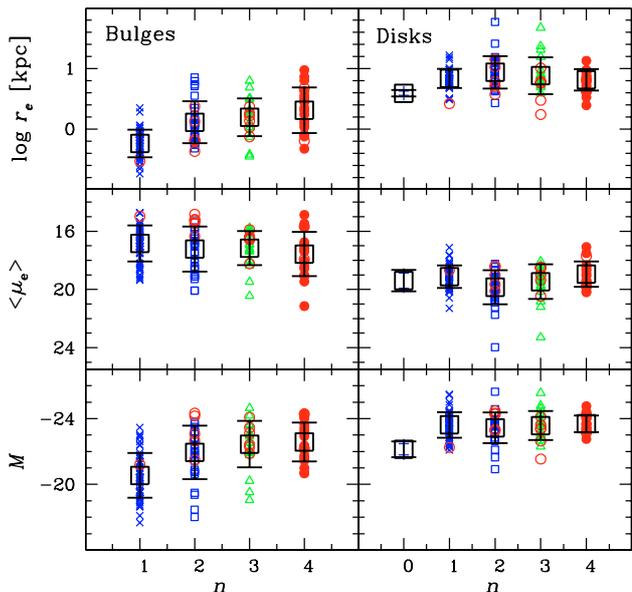
Fig. 4. Bulge and disk structural parameters versus bulge shape index n. The left panels show bulge effective scalelengths (upper panel), mean effective surface brightnesses (middle), and absolute magnitude (lower). The right panels show the same quantities for the disks. Symbols as in Fig. 2.

larger n, significantly different from $n = 1$. This result agrees with other authors (Andredakis et al. 1995; Graham 2001) who found that n tends to increase with decreasing Hubble type. Such a trend could also explain the inconsistency with the results of MACH03 who found no evidence for bulges with $n > 2$, but whose sample contains *only two galaxies earlier than* Sb ($T < 3$).

In what follows, we will examine trends of structural parameters both with the bulge index n and with Hubble type T. The justification for this is that n and T are only weakly correlated (see Fig. 3 and previous work). We want to investigate trends with *bulge shape* as well as with Hubble type since bulges with different n may be intrinsically different (e.g., Carollo 1999; Carollo et al. 2001), independently of the Hubble type of their host galaxies. Therefore, with the aim of singling out the more significant parameter, bulge shape n or Hubble type T, we will analyze trends of photometric parameters with both.

3.4. Bulge/disk parameters versus bulge shape n

The behavior of the structural parameters of bulges and disks as a function of the shape index n of the bulge is illustrated in Fig. 4. Inspection of the figure shows that neither bulge nor disk $< \mu_e >$ vary significantly with n. Obviously, when the bulge μ_e or μ_0 are used (not shown), there is a large variation which is a result of the functional form of the fitting law. The increase of central bulge surface brightness μ_0 with n is ~6 mag arcsec^{-2} in agreement with Khosroshahi et al. (2000a).

r_e^B, instead, increases significantly with n: the left panel of Fig. 4 shows that $n = 1$ bulges have smaller scalelengths than

bulges with higher n^3, while there is no dependence of disk scalelengths on the n of the bulge. The increase of r_e^B with n is consistent with earlier work on ellipticals (Caon et al. 1993), on early-type spirals (Khosroshahi et al. 2000a), and on the later-type spirals in the de Jong sample (de Jong & van der Kruit 1994; Graham 2001). Such a trend was shown to be real, rather than a result of the mutual dependence among n, r_e^B, and μ_e of the bulge fitting law, by Trujillo et al. (2001). Moreover, since the properties of $n = 1$ bulges are shown to differ *with high statistical significance* from their higher n counterparts, it vindicates our method which relies on integer values of n.

The lower panels of Fig. 4 shows M^B and M^D as a function of n. In agreement with earlier work (Andredakis et al. 1995; Graham 2001; MH01; Trujillo et al. 2002), bulges with larger n tend to be more luminous, although with some scatter. Again, we find that $n = 1$ bulges are significantly different from bulges with higher n, being *less luminous* with a significance $>99.9\%$. On the other hand, M^D appears to be independent of n, and significantly less variable in general: the standard deviations of M^B range from 1.2 to 1.6 mag, while those of M^D are considerably smaller, 0.5 to 0.8 mag. The SFBs do not vary with n, and cannot be the cause of the dependence of M^B on n. Exponential bulges are *smaller* and *less luminous* than their higher n counterparts, but roughly the same in terms of mean surface brightness. None of the disk properties ($< \mu_e^D >$, r_e^D, M^D) depends on the n value of the bulge.

3.5. Bulge/disk parameters versus Hubble type

Here we examine the same parameters of the previous section, but now consider their variation with Hubble type T. The relevant graphs are presented in Fig. 5.

The bulge $< \mu_e^B >$ is significantly brighter with decreasing Hubble type; the effect is formally highly significant[4], a new result made possible by the inclusion of the MGH Sa's, and the consequently more ample range in T, as well as by our use of mean SFBs $< \mu_e^B >$, rather than μ_e. Although de Jong (1996) found a similar trend, all bulges were fit with simple exponentials; it was therefore not clear if the effect was real for early-type bulges which are better fit with higher n. No such trend was noted by MH01, although as they point out, their sample extends only to $T = 5$. Also the disk $< \mu_e^D >$ gets brighter with decreasing Hubble type, although the trend is much weaker and not readily discernible in Fig. 5[5]. This also is a new result, which again arises from the large range of Hubble types in our combined sample.

Regarding both bulge r_e^B and disk r_e^D effective scalelengths, the variations with T are small. Although very late-type disks

---

[3] This effect is significant at $>99.9\%$ level (U test). However, the significance is only obtained for $n = 1$ bulges; the differences among r_e^B at other n values are not significant.

[4] Early spiral types ($T \le 2$), intermediate ($2 < T \le 4$) and late ($4 < T \le 6$), and very late ($T \ge 7$) types differ at a significance level of $>99.9\%$, with the exception of late and very late types whose difference is significant at $\sim94\%$.

[5] The increase in disk SFB is formally significant only for early ($T \le 2$) and intermediate ($2 < T \le 4$) types, relative to very late types ($T \ge 7$); the first is $>99.9\%$ significant, while the latter is significant only at a $\sim95\%$ level.
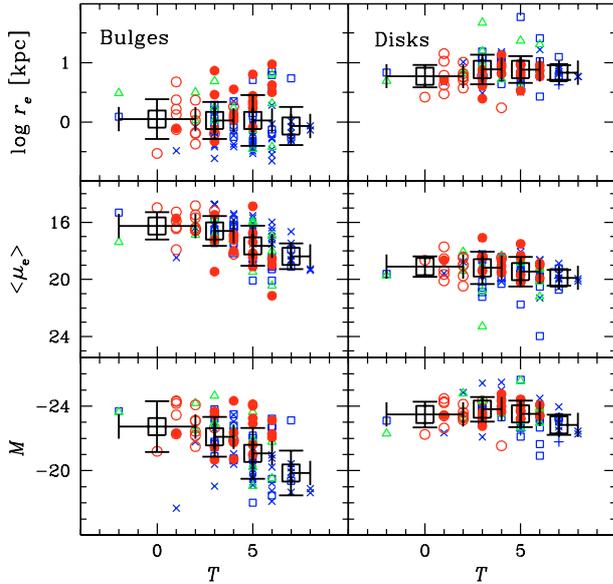
Fig. 5. Bulge and disk structural parameters versus Hubble type T. The left panels show bulge effective scalelengths (upper panel), mean effective surface brightnesses (middle), and absolute magnitude (lower). The right panels show the same quantities for the disks. Symbols as in Fig. 2.
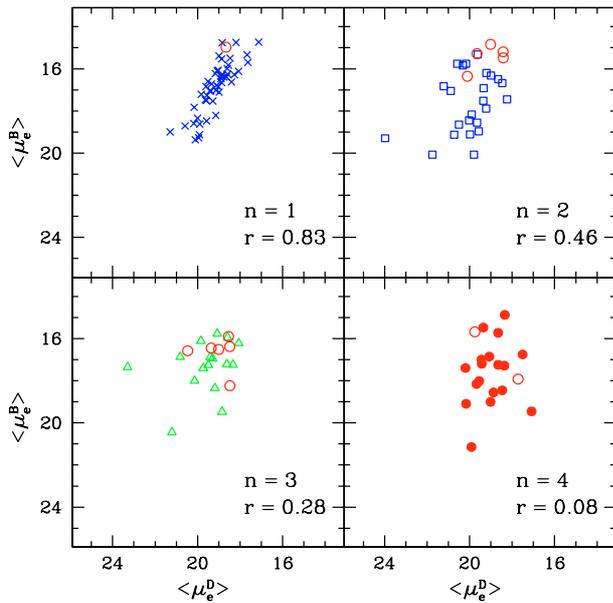

Fig. 6. Bulge versus disk mean surface brightnesses $<\mu_e>$, separately for galaxies with different best n values of the bulge. The correlation coefficients are shown below the values of n.

appear to be smaller than their early-type counterparts, both bulge and disk scalelengths are relatively constant with Hubble type, unlike the variation of bulge r_e^B with n discussed in the previous section. For a given Hubble type, the range spanned by disk properties (M^D, $<\mu_e^D>$, r_e^D) is smaller than that of the bulge (M^B, $<\mu_e^B>$, r_e^B).

The lower panels of Fig. 5 plot the absolute bulge and disk magnitudes M^B and M^D as a function of T. There is a clear trend for the bulge luminosity to decrease going from early
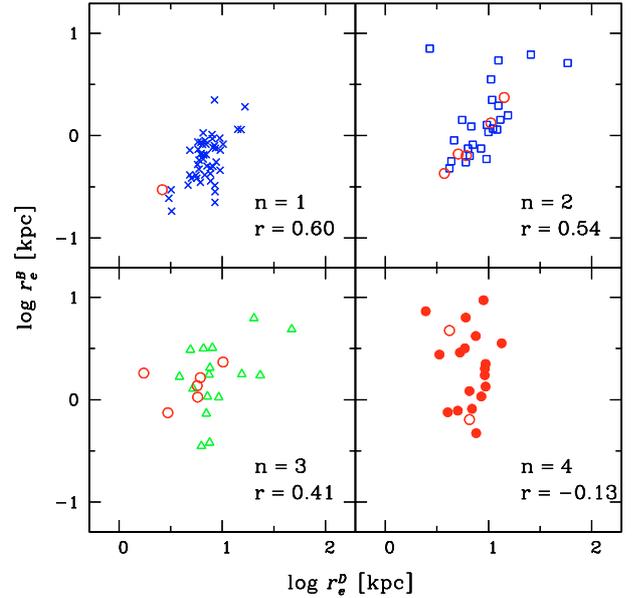

Fig. 7. Bulge versus disk effective scalelengths r_e^B, r_e^D, separately for galaxies with different best n values of the bulge. The correlation coefficients are shown below the values of n.

to very late-type spirals[6]. A similar result was also obtained by MH01. Absolute disk magnitudes do not vary significantly with T, except that very late types $T \geq 7$ are less luminous than all earlier types[7].

3.6. Bulge parameters versus disk parameters

Figures 6–8 illustrate the correlations, separated by n, between the parameters of a bulge and those of its host disk. For all parameters, there is a clear trend for $n = 1$ bulges and disks to be tightly correlated. For $n = 2$, the correlation is somewhat degraded, and by the time $n = 3, 4$, the correlations have all but disappeared. The tendency is evident for mean SFBs (Fig. 6), scalelengths (Fig. 7), and luminosities (Fig. 8).

While this is a new result, one of the main ones of this paper, previous work hinted at something similar. With 1D bulge+disk decompositions of R-band images, and assigning $n = 1$ or 4, Andredakis & Sanders (1994) found a correlation between bulge and disk absolute magnitudes, with the correlations being tighter for systems with $n = 1$ than for $n = 4$ bulges. MH01 found weak correlations between μ_e and μ_0, and with r_e^B and disk scalelength r_e^D, but did not separate or bin the n values; thus the trends evident in our data were diluted in their continuous distribution.

Correlations between bulge and disk radii (Fig. 7) are not new, and have been used to argue for secular evolution as the primary mechanism of bulge formation (e.g., Courteau et al. 1996). Independently of the ratio of radii, which will be discussed in the following section, our data show that the correlation between radii is best for $n = 1$, but degrades steadily toward higher n values. By the time $n = 4$, the correlation has

---

[6] The significance of the trend is >99.9% for all bins, except that $T \leq 2$ and slightly later types are not formally distinguishable.

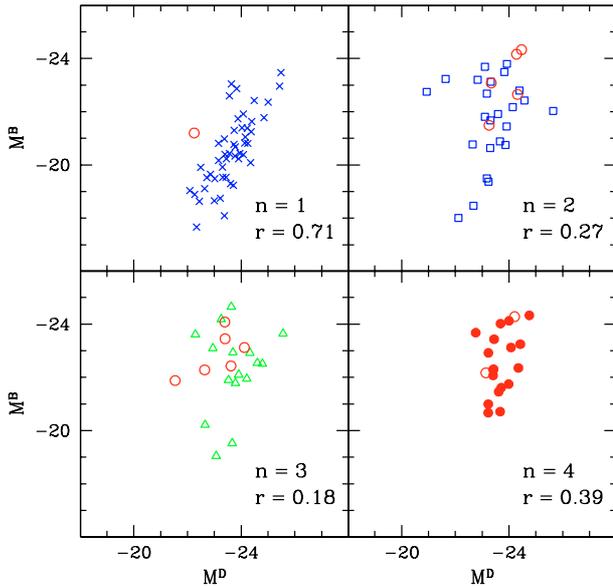[7] Significance is >99% except for $T \leq 2$ which has ~95% significance.

Fig. 8. Bulge versus disk absolute magnitudes M^B, M^D, separately for galaxies with different best n values of the bulge. The correlation coefficients are shown below the values of n.

disappeared completely. If a sample does not contain higher n bulges because of a dearth of early-type spirals, the bulge/disk radii will appear correlated (e.g., MACH03). Our result also agrees with Graham (2001) who found a constant ratio of bulge and disk radii only up to $n \sim 2$. Khosroshahi et al. (2000a) and Scodeggio et al. (2002) also report the existence of such a correlation although they found large scatter; again, this is likely due to the dilution of the correlations when all n values are combined together as done by these authors.

3.7. Bulge/disk scaling relations

Figure 9 shows mean surface brightness $< \mu_e >$ versus effective radius, separately for bulges and disks. We find both bulge and disk $< \mu_e >$ to be well correlated with their effective radii, in the sense that larger bulges and disks tend to be fainter in SFB. This is well known; such correlations have long been found for spiral bulges (Kent 1985; Kodaira et al. 1986; Andredakis et al. 1995), and constitute the "Kormendy" relation for ellipticals (Kormendy 1977; Hoessel & Schneider 1985; Djorgovski & Davis 1989). More recent studies (MH01; Khosroshahi et al. 2000a) also find a similar correlation but with larger scatter. Bulges and disks appear to share the same FP, but occupy distinct, though overlapping, regions of it (Burstein et al. 1997). Combining bulges and disks together, we obtain the regression (shown in the figure) $< \mu_e > = 16.81 + 3.21 \log r_e$, that is $r_e \propto I_e^{-0.78}$, which is consistent with canonical estimates of the FP relation (e.g., Kormendy & Djorgovski 1989): $r_e \propto I_e^{-0.83\pm0.08}$. These are both substantially steeper than the trend reported in MH01 ($r_e \propto I_e^{-1.12}$).

SFBs plotted against scalelengths form an almost face-on view of the FP (e.g., Kormendy & Djorgovski 1989). It can be seen in Fig. 9 that for bulges (top panel) the main scatter in the bulge relation is introduced by $n = 1$ values ($\times$, $r = 0.30$), while the best correlation is for $n = 4$ (filled circles, $r = 0.80$). As in Carollo (1999), for a given radius, $n = 1$ bulges
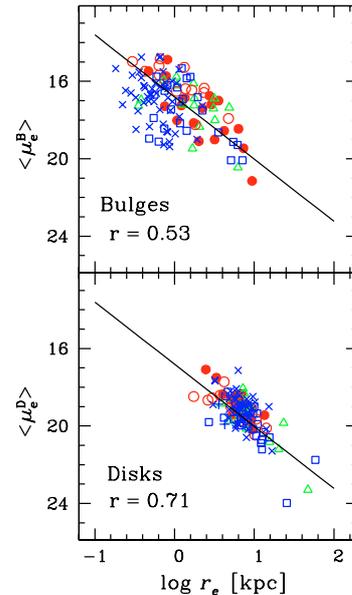

Fig. 9. Bulge mean effective surface brightness $< \mu_e^B >$ versus effective radius r_e^B in kpc (upper panel). Disk mean effective surface brightnesses $< \mu_e^D >$ versus effective radius r_e^D (lower panel). Symbols as in Fig. 2. The best-fit regression (OLS bisector) for all data is shown in both panels.

tend to be fainter than their higher n counterparts. As a whole, disks are significantly better correlated ($r = 0.71$) than bulges ($r = 0.53$ when all n are included). Although this projection of the FP is not ideal for such considerations, these results imply that residuals relative to the FP may be correlated with shape parameters (e.g., Hjorth & Madsen 1995; Prugniel & Simien 1997; Khosroshahi et al. 2000b).

Since scalelength ratios constitute the observational cornerstone for secular evolution scenarios (Courteau et al. 1996, MACH03), we shall discuss this parameter in detail for our data set. Figure 10 shows B/D and r_e^B/r_e^D as a function of n (left panels) and T (right panels). While there is a clear trend for r_e^B/r_e^D to increase with n, there is only a very weak trend for smaller r_e^B/r_e^D with increasing T. For $n = 1$ bulges, we find $< r_e^B/r_e^D > = 0.085 \pm 0.037$ (51 galaxies); for $n = 2 < r_e^B/r_e^D > = 0.15\pm0.10$ (31); for $n = 3 < r_e^B/r_e^D > = 0.21\pm0.16$ (18); for $n = 4 < r_e^B/r_e^D > = 0.32\pm0.32$ (19)[8]. The size ratio increases from $n = 1$ to $n = 4$ by a factor of $\sim$4. The mean value of r_e^B/r_e^D we find for $n = 2, 3$ is consistent with the MACH03 value of 0.22 ± 0.09 for type-I profiles, but this value is more than twice as large as for the $n = 1$ bulges in our sample. Independently of type I vs. type II profiles, we surmise that much of the scatter in the r_e^B, r_e^D relation is due to the mixing of different n bulges. As was seen in Sect. 3.6, the correlation between bulge and disk scalelengths is best for $n = 1$ bulges, then gradually decays to a non-correlation for $n = 4$ (see Fig. 7). In addition to the trend of increasing $< r_e^B/r_e^D >$ with n, the *dispersion also increases with* n: $n = 1$ bulge/disk size ratios have a scatter $\sim$9 times smaller than that for $n = 4$.

---

[8] The difference in effective scalelength ratio among n values is >99.9% significant for $n = 1$ and larger n's, and >99% for $n = 2$ and $n = 4$. $n = 2$ and $n = 3$ ratios do not differ significantly, nor do $n = 3$ and $n = 4$.
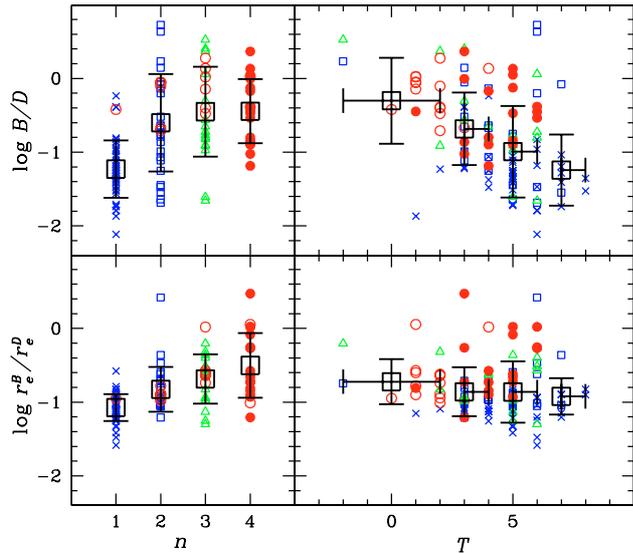
Fig. 10. Bulge and disk effective radius ratios r_e^B/r_e^D (upper panels) and bulge-to-disk luminosity ratios (lower) versus n (left panels) and Hubble type T (right). Symbols as in Fig. 2.

While $< r_e^B/r_e^D >$ depends on n, it is rather independent of Hubble type. The means $< r_e^B/r_e^D >$ for different T bins are statistically indistinguishable, although very late-type spirals ($T \geq 7$) do tend to have $< r_e^B/r_e^D >$ smaller than very early types ($T \leq 2$): 0.12 ± 0.07 (10 galaxies) vs. 0.19 ± 0.13 (19 galaxies). MACH03 also find a slight dependence of $< r_e^B/r_e^D >$ on morphology (~0.20–0.24 from late- to early-type spirals), although the trend is very weak, and not confirmed by Graham (2001), nor with formal significance by our data. Hence, although variations of r_e^B/r_e^D with T are difficult to detect, this ratio changes significantly with the shape of the bulge, implying that the spiral sequence cannot be scale free (cf., Courteau et al. 1996, MACH03). This point will be discussed further in the context of secular evolution scenarios in Sect. 4.

As expected, we find that B/D increases with n and decreases with T, in agreement with previous work (e.g., Andredakis et al. 1995; Khosroshahi et al. 2000a; Graham 2001; MH01). B/D is a criterion for the Hubble classification, so the correlation with T is obvious. The dependence of B/D on n is similar, although of lower significance, than its dependence on T[9]. In any case, the spread of B/D for a given T bin is large, approaching two orders of magnitude, and the looseness of B/D vs. T is rather surprising. It is clear that the Hubble classification reflects complex, multivariate processes, which are not easily quantified.

B/D is larger for early-type spirals because of a brighter $< \mu_e^B >$, since bulge r_e^B, and the disk parameters do not change significantly with T. This is a confirmation of the "iceberg" scenario proposed by Graham (2001). On the other hand, B/D is larger for larger n bulges because r_e^B is larger, since the disk

---

[9] For our data, the significance of the trend with T is formally 99% or greater between all type bins, except for early type spirals ($T \leq 2$) and the next bin ($2 < T \leq 4$), where it is slightly lower (~97%). $n = 1$ bulges have a significantly (>99.9%) lower B/D ratio than higher n values, but the differences among other n values are not formally significant.
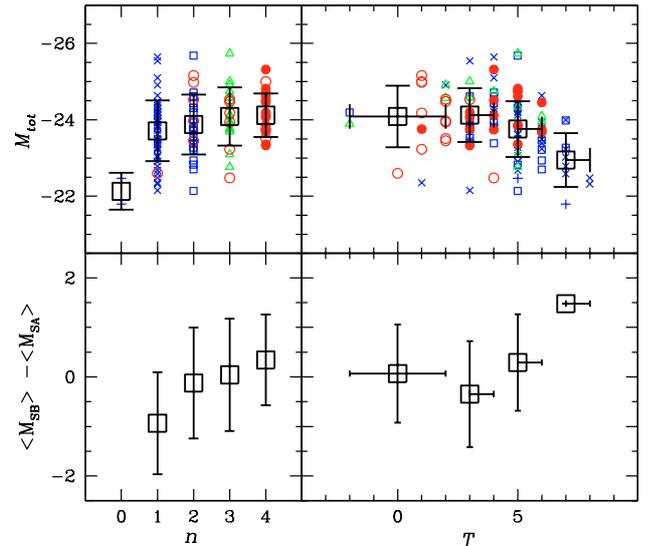

Fig. 11. *Upper panels*: galaxy absolute magnitudes as a function of bulge shape n (left panel) and of Hubble type T (right); symbols as in Fig. 2. *Lower panels*: mean difference in absolute magnitude between strongly barred (SB) and unbarred (SA) galaxies vs. bulge shape index n (left panel) and of Hubble type T (right).

parameters and $< \mu_e^B >$ are roughly constant. When galaxies are divided according to the shape of their bulges rather than their Hubble type, the spiral sequence is seen to be not scale free. It appears therefore that the iceberg scenario proposed by Graham (2001) cannot be only a function of surface brightness. The *shape* of the bulge is a main factor for its increasing prominence with decreasing T; this is true not only because of the variation of r_e^B, but also because of the variation in bulge central surface brightness μ_0^B due to the functional form of the Sérsic law.

3.8. Luminosities

Bearing in mind that our galaxies are rather bright objects, with total galaxy luminosity M^{tot} (H band) $\lesssim -22$, roughly equivalent to M^{tot} (B band)$\lesssim -18$, the sample spans roughly 4 magnitudes, providing some dynamic range for statistical analysis. The upper panels of Fig. 11 shows the total absolute galaxy magnitude (sum of bulge and disk components) vs. bulge shape n (left panel) and Hubble type T (right). As known for some time (e.g., Roberts & Haynes 1994), there is a significant trend of luminosity with Hubble type, in that early-type spirals tend to be more luminous than late types[10]. We find only a weak trend of luminosity with n, since galaxies with $n = 1$ bulges tend to be less luminous than higher n galaxies at the ~95% level, and that the two pure disks are among the least luminous objects in the sample. In any case, the range in luminosities for a given Hubble type bin is large (~3 mag), implying that other variables are at work in addition to T, e.g., DDO classification (van den Bergh 1960).

---

[10] In our sample, this trend is >99% significant for all bins relative $T \geq 7$; the difference in luminosity between $2 < T \leq 4$ and $4 < T \leq 6$ is significant at >95%, although $T \leq 2$ and $2 < T \leq 6$ do not have significantly different luminosities.
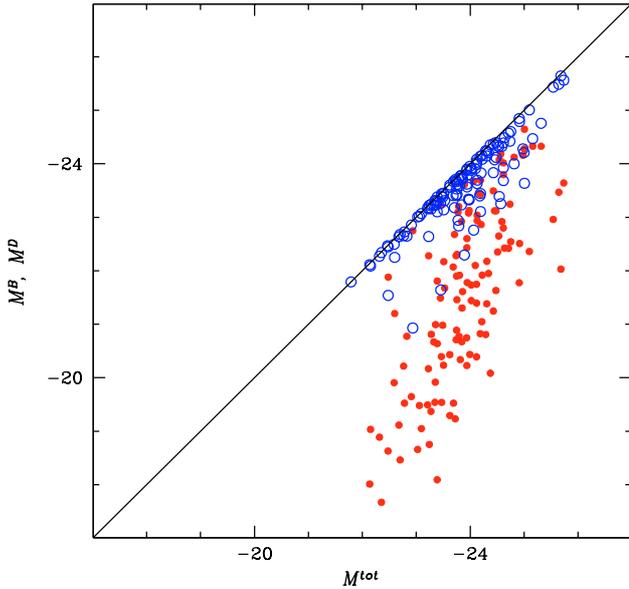
Fig. 12. Bulge M^B (solid circles) and disk M^D (open circles) absolute magnitudes as a function of the total absolute magnitude of the galaxy. Hence, there are two data points for each galaxy.

That earlier Hubble types tend to be more luminous is explained by the analogous trend in bulge luminosity only for $T < 7$, since for these types disks are of roughly the same luminosity. However, for $T \geq 7$ disks tend to be less luminous than those of earlier types, so that the lower total luminosities are due to a lower luminosity of both components, not just of the bulge.

M^B and M^D are plotted against M^{tot} in Fig. 12. The average luminosities of bulge and disk increase with the luminosity of the parent galaxy, independently of the shape n of the bulge. The slope of the correlation is unity for disks and a rather steep 2.5 for bulges. For disks associated with $n = 1$ bulges, the correlation is extremely tight since $M^D \sim M^{tot}$ for these systems. In addition, $M^D \sim M^{tot}$ for the less luminous disk galaxies, while $M^D \sim M^B$ for the most luminous ones. In other words, in the most luminous galaxies, the bulge-to-disk luminosity ratio $B/D \sim 1$.

3.8.1. Influence of bars

We have attempted to assess the influence, if any, of bars on galaxy luminosity, and trends with Hubble type and bulge shape index. In the lower panels of Fig. 11 we plot the difference between the mean absolute luminosities $< M_{SB} >$ and $< M_{SA} >$ of the sample galaxies classified in RC3 as SB (strong bar) and SA (no bar), respectively; the left panel shows this differences plotted vs. n, and the right one vs. T. Inspection of the figure clearly shows that strongly barred galaxies with exponential bulges are significantly more luminous than their unbarred counterparts. Despite the trend of increasing luminosity with n shown in Fig. 11, the *6 strongly barred $n = 1$ galaxies are the most luminous subset in our sample:* $< M_{SB}(n = 1) > = -24.5 \pm 0.9$. There is also a continuous trend toward smaller differences $< M_{SB} > - < M_{SA} >$ with increasing n. However, the same is not true for trends with Hubble type (right panel);

we find no evidence that a strong bar makes galaxies of a given type more (or less) luminous.

4. Discussion

First, we summarize the main results obtained in the previous section.

- Bulge effective scalelengths r_e^B increase with increasing n; $n = 1$ bulges are smaller than those with $n > 1$ (Fig. 4). Neither bulge and disk $< \mu_e >$ nor disk r_e^D vary with n. Bulge luminosity M^B increases with n, while disk luminosity M^D is independent of n (Fig. 4). In particular, exponential bulges are smaller and less luminous than those with $n > 1$.
- Bulge $< \mu_e^B >$ gets brighter as T decreases (Fig. 5). Disk $< \mu_e^D >$ shows a similar, although weaker, trend. Bulge luminosity M^B increases with decreasing T (Fig. 5), but only disks with $T \geq 7$ are significantly less luminous than their early-type counterparts. Neither bulge nor disk scale lengths r_e^B, r_e^D vary significantly with Hubble type (Fig. 5).
- When bulge parameters ($< \mu_e^B >$, r_e^B, M^B) are compared with disk ones ($< \mu_e^D >$, r_e^D, M^D), *in all cases they are tightly correlated for $n = 1$ bulges* (Figs. 6–8). The correlations gradually worsen with increasing n such that $n = 4$ bulges appear *virtually independent* of their disks.
- The scatter in the correlation between bulge $< \mu_e^B >$ and r_e^B (Fig. 9) is shown to depend on bulge shape n; the two parameters are tightly correlated in $n = 4$ bulges ($r = 0.8$), and increasingly less so as n decreases. Disk $< \mu_e^D >$ and r_e^D are well correlated ($r = 0.7$).
- Luminosity ratios B/D are smaller for $n = 1$ bulges than for $n > 1$, and increase with decreasing T, but with a surprisingly large spread (Fig. 10). The value of B/D is governed by the bulge luminosity, since disks have the same average luminosity independently of their shape index n. Bulge-to-disk size ratios r_e^B/r_e^D are also smaller for $n = 1$ bulges, but are independent of Hubble type. The value of r_e^B/r_e^D for $n = 1$ bulges is 4 times smaller than that for $n = 4$, with a spread which is 9 times smaller.
- As already known, early-type spirals tend to be more luminous than late types (Fig. 11); except for $T \geq 7$, this is due to the increasing contribution of the bulge.
- Strongly barred galaxies with exponential bulges are more luminous than their unbarred counterparts. The difference tends to vanish with increasing n. There is no analogous trend with T.

4.1. Bulge formation and evolution

The better correlations of bulge and disk properties for exponential bulges suggest that $n = 1$ bulges and their disks are closely related. The tightness of the relation worsens as n increases, so that when $n = 4$, bulges appear independent of their disks. In contrast, the (Kormendy) relation between bulge SFB and scalelength is very tight for $n = 4$ bulges, and increasingly noisy for lower n values. This implies that $n = 4$ bulges are in some sense more structurally defined than those with lower n.

In the Introduction, we sketched the competing scenarios for bulge formation; here we use the results of our study in

an attempt to distinguish among them. In exclusively "early" bulge formation scenarios, in which the bulge formed before the disk, it is difficult to understand the close relation we observe between exponential bulges and their disks. This relation and its *gradual* degradation as n increases is not easily explained by either the monolithic collapse scenario or CDM merging of primordial disks. If initial conditions were everything, such as in a monolithic collapse, bulge and disk properties should be statistically unrelated. The same would be true if stable disk growth depended on satellite accretion after bulge formation from merging disks, such as in the CDM merging scenarios. It may be that such processes operate for some (higher n) bulges, but they are not a good explanation for the global properties of low n ones. Nor can they explain the gradual worsening of bulge/disk correlations with n.

A close relation between bulges and disks is, however, foreseen by the inside-out formation scheme of van den Bosch (1997). In this scenario, the collapsing halo forms unstable disks which, through bar instabilities, rapidly become "bulges". A disk is able to form only after the bulge becomes large enough to stabilize the ensuing bar. Nevertheless, in this scenario, it is difficult to explain the existence of luminous galaxies with very low B/D ratios. If the presence of a disk depends on the prior buildup of a sufficiently luminous (massive) bulge, then we would not expect to find galaxies with luminous disks and relatively small bulges. Indeed, the existence of pure disk galaxies (~2% of our sample, but see Gavazzi et al. 2000) would appear to contradict this scenario.

A more natural explanation of our observations is the secular evolution scheme in which $n = 1$ bulges are relatively "young" structures, having formed "recently" from their disks through internal gravitational instabilities. This process must be dissipative because of phase-space arguments (e.g., Wyse 1998), but may not exclusively involve bar-driven gas inflow (e.g., Pfenniger & Norman 1990; Combes et al. 1990; Friedli & Benz 1993; Norman et al. 1996). The evolutionary scheme proposed by Zhang in a series of papers (Zhang 1996, 1998, 1999) predicts that "as a galaxy evolves through the spiral-induced collective dissipation process, its surface density distribution (i.e., disk plus bulge) will become more and more centrally concentrated, together with the buildup of an extended outer envelope". Moreover, in a given galaxy, the observed spread in the angular momentum distribution reflects the degree to which secular evolutionary processes have been at work. Since stable stellar systems require a greater degree of velocity anisotropy as n decreases (Ciotti & Lanzoni 1997), $n = 1$ bulges must be kinematically less isotropic than higher n ones. If this anisotropic component is related to tangential motion, and thus to angular momentum, such bulges must be –in the Zhang scenario– *younger*.

Let us therefore hypothesize that exponential bulges are indeed younger than those of higher n, independently of the Hubble type of the galaxy in which they reside. In other words, the first spheroids to be formed from their disks would be bulges with $n = 1$. Such a hypothesis is supported by the blue $V-H$ colors of $n = 1$ bulges, relative to those with $n = 4$ (Carollo et al. 2001). It would also be consistent with the good correlation of exponential bulge properties with those of their

disks as we have seen in Sect. 3.6. If indeed the bulge n increases with time, as predicted by the Zhang models, then our observation that r_e^B and M^B increase with n implies that they also increase with time. The good $n = 4$ correlation of $< \mu_e^B >$ with r_e^B would then be a consequence of their older age and better defined "relaxed" (virialized?) structure, and their consequent better consistency with the FP. The degradation of the correlations between bulge and disk parameters with increasing n would also imply that larger-n bulges are increasingly more distant in time from their disks. In such a scheme, the bulge and disk branches in Fig. 12 could be interpreted as the "evolutionary tracks" of these components.

4.2. The Hubble sequence

Appealing as this picture may be, the trends with Hubble type still need to be explained. Consistently with previous work, we find that higher n values are more common in early-type spirals. Conversely, all (our sample) galaxies with $T \geq 7$ have $n = 1$ bulges. Therefore, there is some indication that n and Hubble type are (albeit weakly) correlated, and may both be associated with age or evolutionary state. Since the degree of evolution is expected to be partly determined by galaxy mass (Zhang 1999), early type spirals which are also more luminous (massive) should in some sense be more evolved than late types. That *surface brightness increases with decreasing Hubble type for bulges and to a lesser extent for disks* is consistent with this expectation. For a given (constant) rate of star formation from the formation epoch to the present day, and a sufficient gas reservoir, we would expect higher stellar surface densities in galaxies which have been forming stars for longer. If, on the other hand, star-formation rates were to depend on (gas+stellar) mass, then we would expect higher mass systems to have higher stellar densities. Either way, it is difficult to reconcile the higher stellar surface densities in early type spirals (Fig. 5) with an earlier evolutionary state (or younger age); they are probably more evolved (i.e., older) systems. Early-type spirals also tend to have lower gas fractions (e.g., Roberts & Haynes 1994) than later types, presumably a result of having converted the available gas into stars.

If late-type spirals ($n = 1$ bulge) are younger than early types (higher n), the question of bars and their effect on evolution must be addressed, since in local samples of galaxies, >75% of very late-type spirals ($T \geq 7$) are barred (Ho et al. 1997; Hunt & Malkan 1999). The excess of bars in very late-type systems may contribute to their morphological evolution as proposed by many groups (e.g., Combes et al. 1990; Pfenniger & Friedli 1991; Friedli & Benz 1993; Hasan et al. 1993; Norman et al. 1996). Numerical models show that bulge-like structures with an exponential $n = 1$ profile can be produced from bar-like perturbations that induce inward radial inflow of disk matter (Pfenniger & Friedli 1991; Zhang & Wyse 2000). Our finding that strongly barred $n = 1$ bulges tend to be more luminous than unbarred ones could reflect such evolution.

Indeed, this bar-driven evolutionary scheme has been advocated by Courteau et al. (1996) and MACH03 to explain the relative constancy of B/D size ratios they find in (the type I

profiles of) their late-type spiral sample. However, they claim that the ratio r_e^B/r_e^D is constant for all spiral types, with the implication that the Hubble sequence is scale free. One of the main results of our study is that several of the trends observed are clearly detected as a function of bulge shape n, rather than T; we interpret this as due to the complex interplay of the spiral classification criteria. With a sample containing few early-type ($T < 2$) spirals, and thus few high-n bulges, several of the trends we found would not be detectable. Hence, we find a wider range of n, in agreement with other groups (Andredakis et al. 1995; MH01; Graham 2001), and also a wider range of r_e^B/r_e^D. We also find that the bulge-to-disk size ratio changes significantly with n. While such variations with n indicate that the Hubble sequence is not scale free, they do not necessarily disprove the secular evolution scenario. However, the scenario must be expanded to include the genesis of bulges with different (higher) n's, together with their distinct properties.

Bar-driven inflow as the unique mechanism of secular evolution may not be sufficient to explain the full range of properties in the Hubble sequence of spirals. The analytical models of Zhang & Wyse (2000) based on viscous evolution of bars find no galaxies with $B/D \sim 1$; their bulges are not sufficiently luminous compared to their disks. Moreover, the secular-evolution simulations of Bouwens et al. (1999) which rely on similar assumptions also produce bulges which are too small and too blue. The collective stellar dissipation scheme proposed by Zhang (1999) may also be insufficient. While qualitatively consistent with our findings, this scheme produces effects (e.g., buildup of central concentration) which are much smaller than those we observe, perhaps because the effects of gas are not included.

Evidently, some other mechanism is needed, such as mergers (e.g., Baugh et al. 1996) or accretion episodes (e.g., Steinmetz & Navarro 2002). However, even mergers in hierarchical clustering scenarios are not able to generate the range of bulge/disk properties in our sample. Scannapieco & Tissera (2003) use hydrodynamical simulations to assess the effects of mergers on disk galaxy structure. While they are able to reproduce the bulge-to-disk size relation for the $n \leq 2$ bulges in our sample and in that of MACH03, the tight correlation of r_e^B/r_e^D for $n = 1$ bulges is not explained. Moreover, they fail to predict the strong increase of r_e^B with n (Fig. 4 and other work), since their models predict the opposite trend. Nevertheless, they successfully reproduce the B/D ratio as a function of bulge shape, although their n values tend to cluster around 1, unlike the early-type spirals in our sample which tend to be best fit by larger n values (Fig. 3). On the other hand Aguerri et al. (2001) are able to reproduce $n = 4$ bulges with satellite accretion, but only with satellites as massive as the bulge itself.

4.3. Conclusions

The hypothesis that emerges from our study is essentially the following:

– Disks are formed first, during an initial collapse, and have properties which depend on the mass and angular momentum of the dark-matter (DM) halo.

– Bulges are then born first as $n = 1$ systems, through secular transfer of disk material to the central regions, probably by bar instabilities.

– With an evolutionary rate that depends on initial conditions (gas+DM mass, angular momentum), n of the bulge increases, with consequent growth of r_e^B, M^B, and B/D, perhaps by means of the collective dissipation mechanism described by Zhang (1999), together with the effects of gas transfer.

– As n gets larger and the bulge builds up, Hubble type gets earlier, with consequent brightening (SFB) of bulges and (less so) disks, and an increase of M^B, B/D.

– Since $n = 1$ bulges are relatively unevolved systems, in a state of formation at the present epoch, they are structurally not as relaxed as larger n bulges, and present a large scatter in the $< \mu_e^B > - \log r_e^B$ (Kormendy) relation. Their stellar luminosity is enhanced by the presence of a strong bar driving the evolution. The $n = 1$ bulges that we see today are those systems which have had long evolutionary times, probably because of their lower luminosity (mass). The evolutionary state of the disk would also be a function of n, since the entire system would be expected to have evolved faster when n is larger.

– Mergers of bulge/disk systems and accretion of gas probably affect the buildup of the bulge, but are probably important only for the creation of high-n bulges.

– The correlation between "evolutionary state indicators" n and T is not expected to be perfect because of the complex nature of spiral classification, and because of variations in galaxy mass, angular momentum, bar strength, gas fraction, dark halo merging history, and perhaps other parameters.

– The gradual growth of a bulge as n increases is implied by the continuity we observe in bulge properties as a function of n. All trends are tight for $n = 1$, and steadily worsen with increasing n, except for the Kormendy relation which is best followed by structurally evolved systems ($n = 4$).

One prediction of such a scenario is a certain spread in stellar age for high-n bulges. Detailed simulations are necessary to assess whether this prediction is in conflict with the level of synchronicity in the star-formation history observed in spheroids (Bower et al. 1992). We also would expect that exponential bulges, prevalent in late-type spirals and closely connected with their disks, would be more dominated by rotation than their higher n counterparts. Low-luminosity spheroids are known to have a higher degree of rotational support than more luminous ones (Davies et al. 1983), so it may be that this is true also for $n = 1$ bulges relative to those of higher n.

Clearly more modelling is needed to understand the full range in properties along the Hubble sequence, and what they imply for bulge formation. However, secular evolution appears to be a strong driver of the Hubble sequence. Our observations are compatible with the hypothesis that n and T are both rough measures of bulge age, and that bulges are, at least initially ($n = 1$), formed secularly from disks.

References

Aguerri, J. A. L., Balcells, M., & Peletier, R. F. 2001, A&A, 367, 428

Andredakis, Y. C., Peletier, R. F., & Balcells, M. 1995, MNRAS, 275, 874

Andredakis, Y. C., & Sanders, R. H. 1994, MNRAS, 267, 283

Balcells, M., & Peletier, R. F. 1994, AJ, 107, 135

Baugh, C. M., Cole, S., & Frenk, C. S. 1996, MNRAS, 283, 1361

Bianchi, S., Ferrara, A., & Giovanardi, C. 1996, ApJ, 465, 127

Bianchi, S., Ferrara, A., Davies, J. I., & Alton, P. B. 2000, MNRAS, 311, 601

Bower, R. G., Lucey, J. R., & Ellis, R. S. 1992, MNRAS, 254, 601

Bouwens, R., Cayón, L., & Silk, J. 1999, ApJ, 516, 77

Burstein, D., Bender, R., Faber, S., & Nothenius, R. 1997, AJ, 114, 1365

Burstein, D., & Heiles, C., 1984, ApJS, 54, 33

Caon, N., Capaccioli, M., & D'Onofrio, M. 1993, MNRAS, 265, 1013

Cardelli, J. A., Clayton, G. C., & Mathis, J. S. 1989, ApJ, 345, 245

Carlberg, R. G. 1986, ApJ, 310, 593

Carney, B., Latham, D., & Laird, J. 1990, Bulges of Galaxies, ed. B. Jarvis & D. Terndrup (Garching: ESO), 127

Carollo, M. C. 1999, ApJ, 523, 566

Carollo, M. C., Stiavelli, M., de Zeeuw, P. T., Seigar, M., & Dejonghe, H. 2001, ApJ, 546, 216

Ciotti, L., & Lanzoni, B. 1997, A&A, 321, 724

Combes, F., Debbash, F., Friedli, D., & Pfenniger, D. 1990, A&A, 233, 82

Combes, F., & Sanders, R. H. 1981, A&A, 96, 164

Courteau, S., de Jong, R. S., & Broeils, A. H. 1996, ApJ, 457, L73

Davies, R. L., Efstathiou, G., Fall, S. M., Illingworth, G., & Schechter, P. L. 1983, ApJ, 246, 41

de Jong, R. S. 1996, A&A, 313, 45

de Jong, R. S., & van der Kruit, P. C. 1994, A&AS, 106, 451

Djorgovski, S., & Davis, M. 1987, ApJ, 313, 59

Eggen, O., Lynden-Bell, D., & Sandage, A. 1962, ApJ, 136, 748

Ferrara, A., Bianchi, S., Cimatti, A., & Giovanardi, C. 1999, ApJS, 123, 437

Freeman, K. C. 1970, ApJ, 160, 811

Friedli, D., & Benz, W. 1993, A&A, 268, 65

Frogel, J. A., Persson, S. E., Matthews, K., & Aaronson, M. 1978, ApJ, 220, 75

Gavazzi, G. 1993, ApJ, 419, 469

Gavazzi, G., Franzetti, P., Scodeggio, M., Boselli, A., & Pierini, D. 2000, A&A, 361, 863

Giovanardi, C., & Hunt, L. K. 1996, AJ, 111, 1086

Giovanelli, R., & Haynes, M. P. 1989, AJ, 97, 633

Giovanelli, R., & Haynes, M. P. 2002, ApJ, 571, L107

Graham, A. W. 2001, AJ, 121, 820

Graham, A.W., & Prieto, M. 1999, ApJ, 524, 23

Graham, A. W., Trujillo, I., & Caon, N. 2001, AJ, 122, 1707

Hasan, H., Pfenniger, D., & Norman, C. 1993, ApJ, 409, 91

Ho, L., Filippenko, Al, & Sargent, W. 1997, ApJ, 487, 591

Hoessel, J. G., & Schneider, D. P. 1985, AJ, 90, 1648

Hjorth, J., & Madsen, 1995, ApJ, 445, 55

Hunt, L. K., Lisi, F., Testi, L., et al. 1996, A&AS, 115, 181

Hunt, L. K., & Malkan, M. A. 1999, ApJ, 516, 660

Jablonka, P., Martin, P., & Arimoto, N. 1996, AJ, 112, 1415

Junqueira, S., & Combes, F. 1996, A&A, 312, 703

Kauffmann, G., White, S. D. M., & Guiderdoni, B. 1993, MNRAS, 264, 201

Kent, S. M. 1985, ApJS, 59, 115

Kent, S. M. 1988, AJ, 96, 514

Kent, S. M., Dame, T. M., & Fazio, G. 1991, ApJ, 378, 131

Khosroshahi, H. G., Wadadekar, Y., & Kembhavi, A. 2000a, ApJ, 533, 162

Khosroshahi, H. G., Wadadekar, Y., Kembhavi, A., & Mobasher, B. 2000b, ApJ, 531, L103

Kodaira, K., Watanabe, M., & Okamura, S. 1986, ApJS, 62, 703

Kormendy, J. 1977, ApJ, 218, 333

Kormendy, J. 1982, ApJ, 257, 75

Kormendy, J. 1993, Galactic Bulges, ed. H. Dejonghe, & H. Habing (Dordrecht: Kluwer), Proc. IAU Symp., 153, 209

Kormendy, J., & Djorgovski, S. 1989, ARA&A, 27, 235

Kormendy, J., & Illingworth, G. 1982, ApJ, 256, 460

Lisi, F., Baffa, C., & Hunt, L. K. 1993, Infrared Detectors and Instrumentation, ed. A. M. Fowler, Proc. SPIE, 1946, 594

Lisi, F., Baffa, C., Biliotti, V., et al. 1996, PASP, 108, 364

Lütticke, R. Dettmar, R.-J., & Pohlen, M. 2000, A&A, 362, 435

MacArthur, L. A., Courteau, S., & Holtzman, J. A. 2003, ApJ, 582, 689 (MACH03)

Möllenhoff, C., & Heidt, J. 2001, A&A, 368, 16 (MH01)

Moriondo, G., Giovanardi, C., & Hunt, L. K. 1998a, A&AS, 130, 81 (MGH)

Moriondo, G., Giovanelli, R., & Haynes, M. P. 1998b, A&A, 338, 795 (Paper II)

Moriondo, G., Baffa, C., Casertano, S., et al. 1999a, A&AS, 137, 101 (Paper I)

Moriondo, G., Giovanelli, R., & Haynes, M. P. 1999b, A&A, 346, 415 (Paper III)

Moriondo, G., Baffa, C., Casertano, S., et al. 2001, A&A, 370, 881 (Paper IV)

Norman, C. A., Sellwood, J. A., & Hasan, H. 1996, ApJ, 462, 114

Ortolani, S., Renzini, A., Gilmozzi, R., et al. 1995, Nature, 377, 701

Peletier, R. F., & Willner, S. P. 1992, AJ, 103, 1761

Pfenniger, D., & Friedli, D. 1991, A&A, 252, 75

Pfenniger, D., & Norman, C. 1990, ApJ, 363, 391

Prugniel, Ph., & Simien, F. 1997, A&A, 321, 111

Rix, H.-W., & Rieke, M. J. 1993, ApJ, 418, 123

Roberts, M. S., & Haynes, M. P. 1994, ARA&A, 32, 115

Scannapieco, C., & Tissera, P. B. 2003, MNRAS, 338, 880

Scodeggio, M., Gavazzi, G., Franzetti, P., et al. 2002, A&A, 384, 812

Sérsic, J. L. 1968, Atlas de galaxias australes, (Córdoba: Observatorio Astronómico de Córdoba)

Shaw, M. 1993, MNRAS, 261, 718

Steinmetz, M., & Navarro, J. F. 2002, New Astron., 7, 755

Trujillo, I., Asensio Ramos, A., Rubiño-Martín, J. A., et al. 2002, MNRAS, 333, 510

Trujillo, I., Graham, A. W., & Caon, N. 2001, MNRAS, 326, 869

van den Bergh, S. 1960, Publ. David Dunlop Obs., 2, 159

van den Bosch, F. C. 1998, ApJ, 507, 601

de Vaucouleurs, G., de Vaucouleurs, A., Corwin, H. G., et al. 1991, Third Reference Catalogue of Bright Galaxies (New York: Springer-Verlag) (RC3)

Widrow, L. M., Perrett, K. M., & Suyu, S. H. 2003, ApJ, 588, 311

Wyse, R. F. G. 1998, MNRAS, 293, 429

Zhang, X. 1996, ApJ, 457, 125

Zhang, X. 1998, ApJ, 499, 93

Zhang, X. 1999, ApJ, 518, 613

Zhang, B., & Wyse, R. F. G. 2000, MNRAS, 313, 310